Structure and magnetic properties of oxygen-stabilized tetragonal Ni nanoparticles prepared by borohydride reduction method

Aparna Roy and V. Srinivas*
Department of Physics and Meterology, Indian Institute of Technology, Kharagpur 721302, India

S. Ram
Materials Science Center, Indian Institute of Technology, Kharagpur 721302, India

J. A. De Toro†
Departamento de Fisica Aplicada, Universidad de Castilla-La Mancha, 13071 Ciudad Real, Spain

U. Mizutani
Department of Crystalline Materials Science, Nagoya University, Furo-cho, Chikusa-ku, Nagoya, Aichi-ken 464-8603, Japan
(Received 1 July 2004; revised manuscript received 1 November 2004; published 31 May 2005)

We report a comprehensive study on the structure and magnetic properties of ultrafine Ni nanoparticles prepared by the borohydride reduction method. A spontaneous surface oxide layer of NiO encapsulates the Ni particles, as these have been prepared under ambient atmosphere. From the x-ray diffraction (XRD) pattern, the "as-prepared" sample has been identified as Ni in a tetragonal crystal structure, stabilized by the incorporation of oxygen atoms in the Ni lattice. On annealing this sample in air at different temperatures, the XRD patterns showed an interesting feature: unexpected fcc Ni peaks appeared together with the usual NiO peaks. Anomalous behavior is also observed in the *M-H* curves, with the as-prepared sample showing a linear response with field and low values of magnetization and the annealed samples showing ferromagnetism with large coercivity (290 Oe) and high magnetization values. These surprising and seemingly contradictory observations have been coherently explained on the basis of a proposed phenomenological model. Furthermore, we attribute the observed low magnetization values of the as-prepared sample to an antiferromagnetic superexchange interaction between some of the Ni atoms, mediated by the dissolved oxygen atoms in the Ni lattice.

DOI: 10.1103/PhysRevB.71.184443 PACS number(s): 81.07.−b

I. INTRODUCTION

Nanosized particles of ferromagnetic metals, such as Fe, Co, and Ni, are the focus of growing interest in recent years because of both the richness of their physical properties and potential applications in diverse areas, such as magnetic recording media, sensors, ferrofluids, and catalysts.[1,2] A considerable amount of work has been done since the last decade on various nanoparticle (NP) systems, such as metal particles, transition metal oxides (CrO_2, Cr_2O_3, NiO), heterogeneous granular alloys containing Cu or Ag with a transition metal (Fe-Cu, Co-Cu, Fe-Ag, Co-Ag,[3] Ni-Ag); ferrites, such as γ-Fe_2O_3,[4] Ni ferrite[5] ($NiFe_2O_4$); mixed systems, such as Fe-Pt,[6] Co-Pt,[7] Ni-Pd; and transition metal-boron alloys, such as Fe-B, Co-B, Ni-B,[8,9] Fe-Ni-B,[10] and Co-Ni-B.[11] In addition, there have also been studies on transition metal-transition metal oxide systems (Fe-FeO,[12,13] Co-CoO[14]) and transition metal-insulator systems, such as Fe, Co, or Ni dispersed in SiO_2 (Refs. 15 and 16) or Al_2O_3 (Refs. 17 and 18) matrices. The voluminous work covered a vast expanse of theoretical and applied physics with topics such as interparticle interactions and their modeling, Monte Carlo simulations of spin configurations in the NPs, distinction between superparamagnetic and spin-glass regimes, devitrification of Ni-B alloys, origin of magnetic anomalies in NiO nanoparticles, and surface effects on the magnetization of NPs to name a few on the theoretical side. On the application front, the studies mainly dealt with the efficacy of the materials as GMR (giant magnetoresistance) or TMR (tunneling magnetoresistance) sensors and high-density magnetic recording media.

It is an irrefutable fact that a passivating oxide layer on ferromagnetic metal NPs plays a significant role in modifying the global magnetic properties of the particles. For example, the existence of broken bonds, the lack of structural periodicity, and the presence of competing magnetic interactions at the surface can produce[19] spin-canting and spin-glass–like behavior in the disordered surface oxide layer and subsequent reduction of the net magnetization of the NP. Not only an oxide layer, the magnetization of nanocrystalline ferromagnets are also reported to be highly sensitive to oxygen contamination.[20] A rough estimate[21] shows that every oxygen atom destroys the contribution of one Ni atom to ferromagnetism and leads to a strong decrease of magnetization. The surface oxide layer and absorbed oxygen in magnetic NPs thus merit an in-depth and exhaustive study.

Although thermal oxidation of bulk samples and thin films has been studied in considerable detail, the oxidation of fine metal particles has not been a widely studied subject. Some isolated but informative studies on transition metal-transition metal oxide systems[22,23] have, of course, been performed in the recent past. Reports on oxidation kinetics of Ni particles prepared by vapor-deposition techniques also exist in the literature. However, it is still not clear how the magnetic properties get affected when the Ni NPs transform to NiO via oxygen diffusion. In fact, Ni has been a less studied metal in comparison to Fe (Ref. 22) and Co.[23,24] Most studies

on Ni have been concentrated on pure Ni (Refs. 25 and 26) or pure NiO (Refs. 27–29) nanoparticles or Ni-B alloys, with no systematic studies to date on the evolution (as a function of annealing temperature) of structure and magnetic properties as Ni gets transformed to NiO on annealing in air. Such a study is both academically enlightening and technologically useful, since at a particular annealing temperature, Ni-NiO composites are formed. These have presently become quite attractive for applications and show promising properties, especially in the field of electrochemical capacitors.[30] The prime requirements for an electrochemical capacitor are an inexpensive porous metal oxide material having extensive surface area, good conductivity, and high specific capacitance. Liu *et al.*[30] claim that porous NiO-Ni composite thin films having a surface area $>30\ m^2/g$, porosity in the range of 10–80%, and a mean grain size between 2 and 100 nm are very promising candidates for electrochemical capacitors.

In order to study the evolution of structure and magnetic properties as Ni gets transformed to NiO on annealing, nanoparticles of Ni were first prepared by a chemical reduction method, namely, the reduction of a Ni salt solution by an alkali metal borohydride.[23,31–36] This unique reduction technique has been used extensively for the production of nanoscale metal or metal boride particles. Earlier workers have investigated the effect of different reaction media and environments on the end product of this reaction. These studies suggest that Ni/NiO or Ni/Ni-B can be obtained as the final product when the reaction is carried out in aqueous medium and in air. However the reaction mechanism still remains debated. In addition to this, in earlier investigations, the structure of the as-prepared sample (i.e., end product) could not be determined from either XRD pattern or any other structural analysis. Recently, Roy *et al.*[37] have discussed the reaction mechanism in ambient atmosphere and subsequently demonstrated the effect of oxygen on the structure of the final product. They have identified the end product to be Ni in a tetragonal crystal structure, stabilized by the incorporation of O atoms in the Ni lattice. However these samples were prepared using Ni salt solutions of relatively high concentration (1 M), whereas most of the earlier studies concentrated on low concentration (millimolar) solutions.

In this paper we present a comprehensive study of the structure and magnetic properties of Ni NPs obtained by reducing a 0.1 M aqueous $NiCl_2$ solution (low concentration) by the borohydride reduction method. The structure of the as-prepared sample is established to be the same as that in our earlier report[37] on samples obtained from high-concentration $NiCl_2$ solutions. A plausible explanation of how interstitial oxygen atoms affect the magnetization of the NPs is given. Furthermore we have also studied in some detail how the structure and magnetic properties evolve when the samples are subjected to thermal treatment in air. To corroborate our results, we have also performed measurements on samples obtained from a 0.5 M aqueous $NiCl_2$ solution, i.e., another low-concentration solution. The results of both of these samples (henceforth written as 0.1 M and 0.5 M samples) show similar trends. Finally, a phenomenological model has been proposed that explains consistently all results obtained in the present study.

II. EXPERIMENTAL DETAILS

Fine particles of Ni were prepared by reducing the nickel salt $NiCl_2 \cdot 6H_2O$ with sodium borohydride ($NaBH_4$) as reducing agent. The reaction was carried out in an aqueous medium at room temperature. 200 ml of a 1 M solution of $NaBH_4$ was added dropwise over a period of 1 h to 500 ml of a 0.1 M $NiCl_2 \cdot 6H_2O$ solution in a beaker, with constant magnetic stirring. An instantaneous exothermic reaction ensued with the formation of black slurries of Ni NPs and evolution of H_2 gas. Average temperature of the solution rises by 10–20 K. However the dropwise addition of $NaBH_4$ controls the reaction and maintains the average temperature of the solution at approximately room temperature. It seems that the reaction in air monitors *in situ* surface reaction of the resulting Ni sample with H_2O in the solution, forming a stable spontaneous surface oxide (SSO) layer of NiO as an integral part of each individual Ni particle.

After the $Ni^{2+} \rightarrow Ni$ reaction, the sample (slurries of Ni NPs) was filtered and washed thoroughly with distilled water to remove all residual ions from the reaction mixture. This was followed by washing with acetone, to remove the water. We found that a thorough washing is essential to get rid of unwanted impurities, such as elemental boron and its compounds with Ni. The recovered powder was dried in vacuum, at $\sim$10 mbar pressure, at room temperature. The sample so obtained is black in color and stable in ambient atmosphere. The same procedure was followed for obtaining samples from the 0.5 M $NiCl_2$ solution. Annealing in air at temperatures of 573, 773, and 973 K for 1 h is used to analyze the oxidative reaction of the Ni core through the NiO shell as diffusion barrier. A pure fcc Ni powder results on annealing the sample in H_2 gas at 973 K or higher temperature.

The crystalline structure of the sample was studied by x-ray diffraction using a Philips P.W. 1718 x-ray diffractometer with filtered Cu Kα radiation of wavelength $\lambda = 0.154\ 18$ nm. Microstructure was studied with a JEM 2000cx transmission electron microscope (TEM). *In situ* elemental analysis with an electron microprobe analyzer confirms the absence of Na^+ and Cl^- by-product impurities. The thermal stability (DTA/TGA) of the sample was studied using a Perkin Elmer Instruments thermogravimetric/differential thermal analyzer, in the temperature range 358–1073 K, with a heating rate of 10 K/min and in a flow of Argon gas at 100 ml/min.

The room temperature *M-H* curves were measured with a vibrating sample magnetometer using magnetic fields up to 14 kOe. The field-cooled/zero-field-cooled (FC/ZFC) curves and the *M-H* curves at 5 K were measured with a SQUID magnetometer (Quantum Design). Thermal variation of ac susceptibility was measured using a conventional mutual inductance bridge.

III. RESULTS AND DISCUSSION

A. X-ray diffraction and microstructure

Figure 1 compares the x-ray diffractograms of the as-prepared and annealed powders of the 0.1 M sample. The diffractograms are indicative of a crystalline structure with

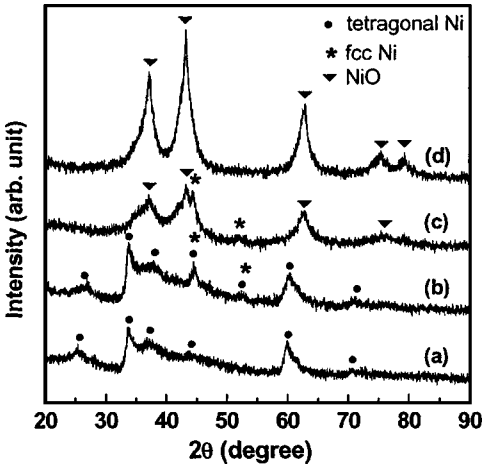

FIG. 1. X-ray diffractograms of 0.1 M sample: (a) as-prepared and after annealing in air at (b) 573 K, (c) 773 K and (d) 973 K for 1 h.

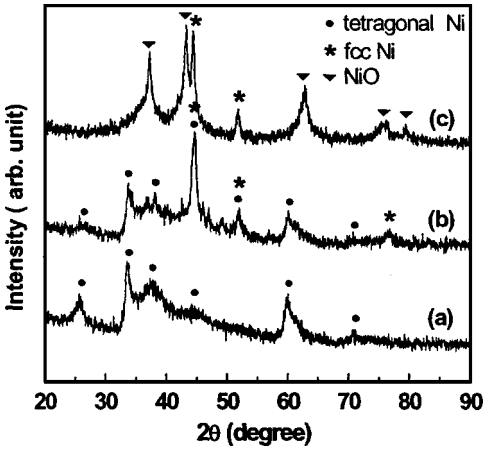

FIG. 2. X-ray diffractograms of 0.5 M sample: (a) as-prepared and after annealing in air at (b) 573 K and (c) 773 K for 1 h.

some degree of disorder, which could stem from surface layers. A slight change in the form of two extra peaks at $2\theta = 44.5°$ and 51.85°, is observed on annealing the as-prepared sample at 573 K. The effect is more pronounced in the case of 0.5 M sample as shown in Fig. 2. Further annealing at 773 K shows prominent peaks of NiO along with the two peaks of fcc Ni at 2θ values of 44.5° and 51.85°. Finally, the sample annealed at 973 K is completely converted to NiO and shows only broad NiO peaks. The most intriguing aspect of the XRD patterns is the appearance of fcc Ni peaks on annealing in air at 573 and 773 K. Similar features are also observed in the XRD patterns of the 0.5 M sample (Fig. 2).

Diffraction patterns (a) and (b) of as-prepared and 573 K annealed samples of Figs. 1 and 2 do not correspond to fcc, Ni and no attempts have been made to date by earlier investigators[31,36] to identify the structure. As discussed in our previous report,[37] we find that these patterns are the modified patterns of the usual fcc Ni metal. The most intense peaks (intensity $I_p = 100$ units) in Figs. 1(a) and 1(b) occur at interplanar spacings of 0.2667 and 0.2659 nm, respectively. In the usual Ni metal,[38] the most intense peak (111) lies at $d = 0.2034$ nm with the second most intense one (200) at $d = 0.1762$ nm ($I_p = 42$ units). We have indexed the peaks of diffractograms (a) and (b) in Fig. 1, assuming a tetragonal crystal structure (Table I) with space group 14/mcm. The lattice parameters are $a = 0.4920$ nm, $c = 0.5355$ nm for the as prepared sample and $a = 0.4885$ nm, $c = 0.5345$ nm for the sample annealed at 573 K. Similar indexing can be done on the XRD pattern of the 0.5 M sample. We propose that a tetragonal Ni-O_β lattice is derived from the fcc Ni lattice by the incorporation of O atoms at the interstitial positions of the latter. A considerable amount of this dissolved oxygen in the sample modifies the usual fcc crystal structure of virgin Ni particles, straining and hence making them tetragonal. A detailed discussion can be obtained in Ref. 37.

The O atoms in Ni-O_β become mobile at temperatures above 573 K and, when annealed in air, induce phase transformation according to the equation,

$$\text{Ni - O}_\beta = \text{cubic} - \text{Ni}_{1-\beta} + \beta\text{NiO}$$

The removal of the dissolved oxygen leads to the release of strain from the Ni lattice and thereby to the return of Ni back to its fcc structure. Finally an efficient reaction with O_2 from air occurs on annealing at 973 K, resulting in the formation of fine NiO particles of crystallite size 5 nm, as estimated

TABLE I. X-ray-diffraction pattern of Ni nanocrystals of tetragonal crystal structure. The lattice parameters are given below (as-prepared powers: $a = 0.4920$ nm, $c = 0.5355$ nm; 573 K annealed powers: $a = 0.4885$ nm; $c = 0.5345$ nm).

As-prepared			573 K Annealed		
d_{hkl} (nm)[a]	Intensity[b]	(h k l)	d_{hkl} (nm)[a]	Intensity[b]	(h k l)
0.3493 (0.3479)	65	(1 1 0)	0.3440 (0.3454)	33	(1 1 0)
0.2667 (0.2677)	100	(0 0 2)	0.2659 (0.2672)	100	(0 0 2)
0.2448 (0.2460)	78	(2 0 0)	0.2430 (0.2442)	73	(2 0 0)
0.2055 (0.2035)	52	(2 1 1)	0.2031 (0.2022)	73	(2 1 1)
			0.1762 (0.1781)	25	(0 0 3)
0.1543 (0.1556)	82	(3 1 0)	0.1535 (0.1545)	58	(3 1 0)
0.1332 (0.1322)	26	(3 2 1)	0.1323 (0.1313)	27	(3 2 1)

[a]The figures in parentheses are the d_{hkl} values calculated from the respective lattice parameters of the samples.
[b]The relative intensities are normalized assuming 100 units of intensity for the most intense peak.

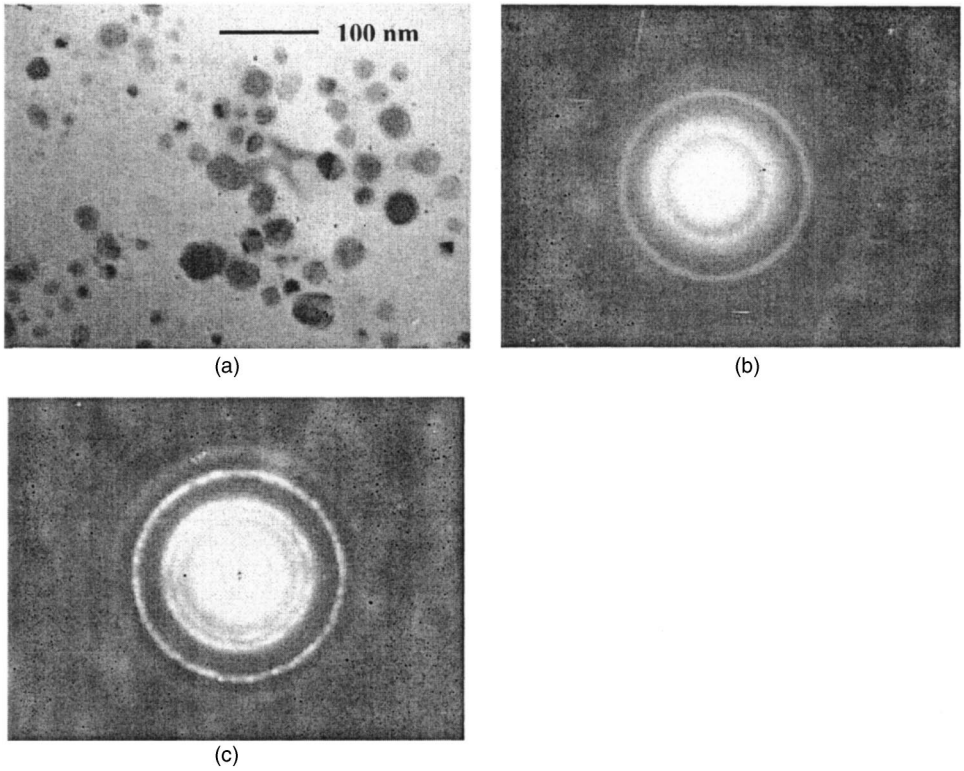

FIG. 3. (a) TEM micrograph and (b) corresponding electron diffractogram of 0.1 M, 573 K, air-annealed sample. (c) Significant modification due to surface oxidation is seen in the electron diffractogram of the 773 K annealed sample.

from x-ray-diffraction line broadening [Fig. 1(d)] using the Scherrer equation. This, however, is only a rough estimate of the crystallite size because the Scherrer formula does not consider any peak broadening due to strain. An important point to be noted here is the simultaneous existence of Ni in both tetragonal and fcc phases, as portrayed by the diffraction patterns of the 573 K annealed sample in Figs. 1(b) and 2(b). For fcc Ni, the peaks at $2\theta = 44.5°$ and 51.85° correspond to reflections from (111) and (200) planes, respectively, whereas for tetragonal Ni, the same peaks appear because of reflections from (211) and (003) planes (Table I).

Isolated, spherical particles of average diameter 20 nm are seen in the TEM micrograph of the 0.1 M as-prepared powder [Fig. 3(a)]. The electron diffractograms of the 573 K and the 773 K annealed samples [Figs. 3(b) and 3(c)] show ring patterns typical of nanocrystalline materials. However, a significant crystal growth and/or elimination of crystal defects seems to have occurred in the 773 K annealed sample, as is evident from the sharpness and the higher intensity of the rings in Fig. 3(c). Five distinct rings are observed in the electron diffractogram in Fig. 3(c) at d_{hkl} values of 0.2413, 0.2082, 0.2036, 0.1768, and 0.1478 nm. The first two and the last ring are due to NiO with reflections from (111), (200), and (220) planes, whereas the third and fourth ring are due to reflections from Ni (111) and (200) planes, in close conformity with x-ray-diffraction results.

B. Thermal analysis and phase stability

It is evident from the XRD patterns (Figs. 1 and 2) that the transformation of Ni nanoparticles from the tetragonal to fcc phase takes place at some temperature intermediate to 573 and 773 K. To find out precisely at what temperature this happens, we have studied the thermal evolution of the phases by both differential thermal analysis (DTA) and thermo gravimetric analysis (TGA) techniques. Figure 4 shows the DTA and TGA profiles of the 0.1 M sample. A sharp endothermic peak at 661 K and two exothermic peaks at 545 and 700 K are observed in the profile. The broad exothermic peak at 545 K is probably due to the crystallization of any amorphous species present in the surface layers.

The endothermic peak at 661 K appears possibly because of the desorption of the dissolved oxygen from the tetragonal lattice. This leads to the collapse of the tetragonal structure of the Ni nanoparticles and subsequent crystallization of the

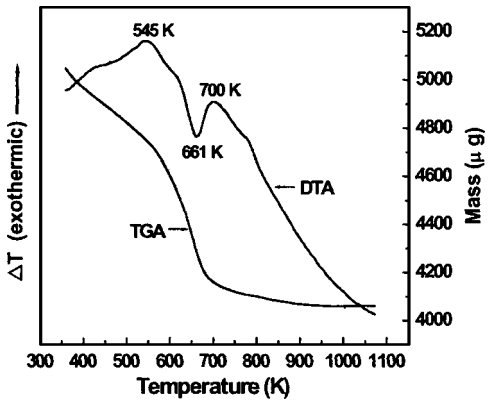

FIG. 4. DTA and TGA profiles of the 0.1 M sample obtained with a heating rate of 10 K/min in argon atmosphere.

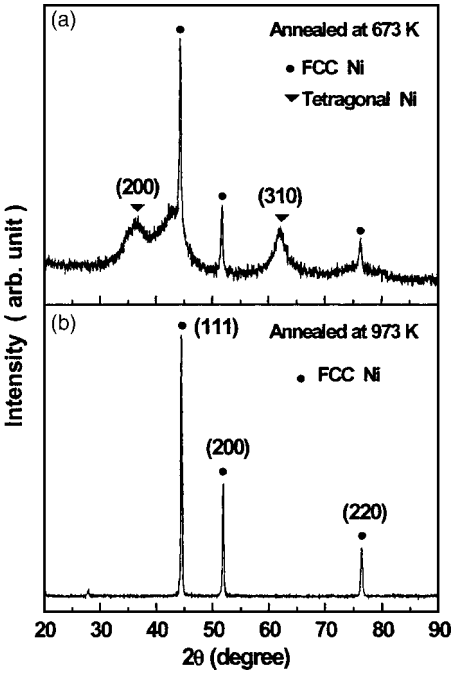

FIG. 5. X-ray diffraction patterns of 0.1 M sample annealed in Argon gas for 1 h at (a) 673 K and (b) 973 K.

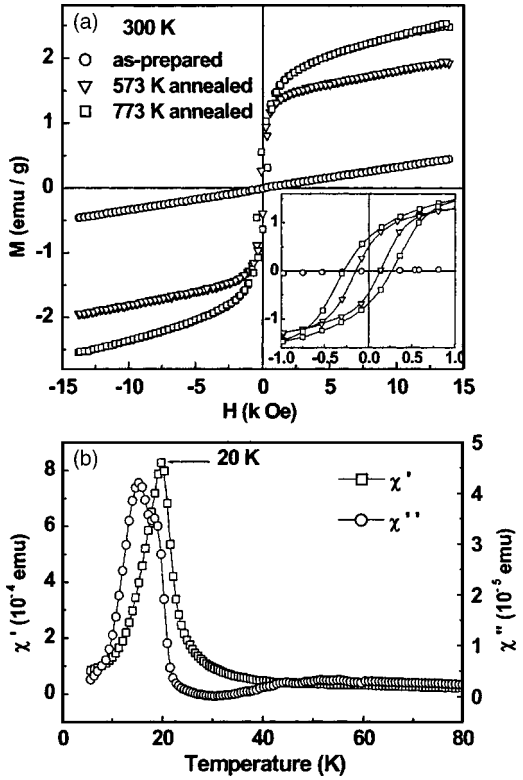

FIG. 6. (a) Magnetization (M) as a function of applied field (H) at 300 K, for the 0.1 M sample. Inset: An expanded view of the plots, clearly showing hysteresis. (b) Temperature dependence of the real (χ') and imaginary (χ'') components of ac susceptibility at an excitation frequency of 10 kHz.

fcc phase. The sharp exothermic peak at 700 K signals the release of strain energy and the transformation to this phase. The TGA curve shows a steep fall with a 20% weight loss in the sample at 700 K, confirming further, the desorption of the dissolved oxygen.

As an added support to our proposition of tetragonal Ni and its transformation to fcc phase, the XRD patterns of the 0.1 M sample annealed in Argon at 673 and 973 K are presented in Fig. 5. The 673 K annealed sample shows peaks of fcc Ni along with two other peaks at $2\theta = 36.3°$ and 61°. These belong to tetragonal Ni and are due to reflections from (200) and (310) planes, respectively, (Table I). Thus at 673 K, the sample is in the final stages of phase transformation with the coexistence of major fcc and minor tetragonal phases. Finally, as portrayed in the DTA profile, this transformation gets completed at 700 K so that any further annealing in Argon or H_2 at higher temperatures, shows only fcc Ni peaks [Fig. 5(b)].

Thus the XRD pattern and DTA profile of the 0.1 M sample corroborate each other and lends credence to our conjecture that tetragonal Ni is formed by the incorporation of oxygen atoms in the Ni lattice. Similar behavior is also seen in the 0.5 M sample.

C. Magnetic properties

We split up our analysis of the magnetization results into two parts. Section III C 1 discusses the room temperature magnetic state of the samples and explains the nonsaturating, hysteretic magnetization. Section III C 2 gives a plausible explanation of the low magnetization values of the as-prepared sample.

1. Nonsaturating and hysteretic magnetization

The magnetic state of the as-prepared and annealed samples has been assessed through room temperature (300 K) magnetization data. Figure 6(a) shows the M-H curves of the 0.1 M as-prepared and annealed samples at room temperature. These measurements give information about the presence and distribution of oxides in nanostructured materials.[39] The data shows some interesting features: (i) a sharp increase in magnetization at low fields, followed by a linear nonsaturating behavior for samples annealed in air; (ii) increase in magnetization, remanent magnetization (M_r), and coercivity (H_c) values as the annealing temperature is increased to 773 K; and (iii) in the case of the as-prepared sample, very low magnetization values and a linear magnetization response with applied field. A similar behavior is also observed in the room-temperature M-H plot [Fig. 7(a)] of the 0.5 M as-prepared sample, whereas the annealed sample exhibits larger values of magnetization. As expected, the magnetization of the 0.5 M annealed sample is larger in comparison to the corresponding annealed sample of the 0.1 M series.

In order to gain more insight into the nature of the as-prepared sample, M versus T curves for the 0.5 M powder were measured in zero-field-cooling (ZFC) and field-cooling (FC) conditions for an applied field of $H = 100$ Oe, from 300 to 5 K [Fig. 7(b)]. The measurements show an irreversibility in the FC and ZFC curves, hinting at the metastable nature of the sample magnetization. The temperature of the maximum in the ZFC curve (here 18 K) is, in general, for single domain particles, denoted as the average blocking

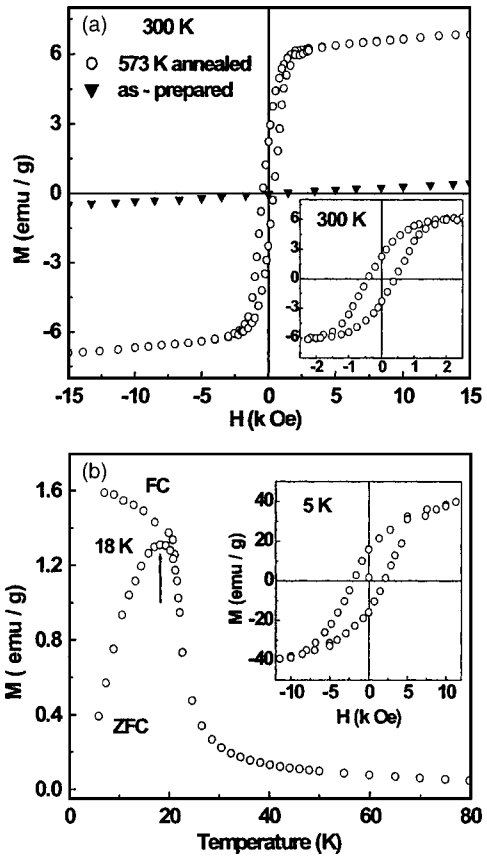

FIG. 7. (a) *M-H* plot at 300 K for the 0.5 M sample. Inset: Expanded view of the plot for the 573 K annealed sample. (b) Magnetization of FC and ZFC particles of the as-prepared sample in 100 Oe applied field, as a function of temperature. Inset: *M-H* plot at 5 K, showing hysteresis.

temperature T_B, below which the sample is seen as a stable ferromagnet. This is manifested by hysteresis in the M versus H plot at 5 K [Fig. 7(b), inset]. However, such behavior has also been observed in systems, such as bulk alloys, having competing exchange interactions. The 0.5 M as-prepared sample may be identified as being superparamagnetic at room temperature and from the complete resemblance of the *M-H* plots of the 0.1 and 0.5 M as-prepared samples, we can arrive at the same conclusion for the former. Alternatively, the ac susceptibility measurements of the 0.1 M sample (Fig. 6(b)) at an applied frequency of 10 kHz, too shows a peak at 20 K in the χ'' versus T plot, suggesting a possibility of the sample being superparamagnetic. However, a detailed study of the magnetization dynamics and ac susceptibility experiments is required to confirm this magnetic phase.

The magnetization of the annealed samples displayed in Fig. 6(a) does not saturate. At lower fields the magnetization shows a rapid increase with field, followed by a curvature and then by a high-field linear behavior, suggesting the existence of two different magnetic phases in the sample—a ferromagnetic and a weakly magnetic (superparamagnetic or antiferromagnetic) phase. The presence of the ferromagnetic phase is established by hysteresis [Fig. 6(a) inset] and its evolution is observed through the increase in values of M_r and H_c from 0.458 emu/g and 148 Oe in the 573 K annealed sample to 0.693 emu/g and 289 Oe in the 773 K annealed sample. Since XRD shows no trace of any phase other than Ni and NiO in the annealed samples, the observed two magnetic components can be attributed to the presence of either (i) individual Ni and NiO particles in the samples or (ii) Ni-NiO particles in a core-shell morphology with the NiO acting as a passivating layer. The steps taken for the synthesis of the particles do not favor (i). Furthermore, the increase of magnetization values on annealing in air cannot support such a phase because annealing is likely to cause transformation of all Ni particles to NiO and subsequent reduction in magnetization. The magnetization features can, however, be coherently explained by considering a core-shell model, where each particle has a magnetically heterogeneous structure with a ferromagnetically ordered Ni core and a spin-disordered shell of NiO or any other paramagnetic impurities in the form of nickel borides. However, no significant borides could be detected in the XRD patterns even after annealing in air/argon at 973 K for 1 h. We point out here that the existence of a pure antiferromagnetic phase in the shell can be ruled out since nanoscale NiO is not a perfect antiferromagnet but has a net magnetic moment due to uncompensated surface spins,[40] although in the interior the spins are likely to be compensated. Due to thermal agitation, these exchange-decoupled surface spins point in rather random directions, imparting to the shell surface a superparamagnetic character.

Relatively large coercivities of 148 and 289 Oe are observed at 300 K for samples annealed at 573 and 773 K, respectively [Fig. 6(a) inset]. We attribute the observed large coercivities to the influence of interface anisotropy. The Ni core and NiO shell nanostructure can be described as a magnetic bilayer with spherical geometry. It is then reasonable to anticipate that the NiO shell acts as a pinning layer as in spin valve structures, pinning the core spins near the interface of the Ni core and NiO shell, via exchange interactions. This prevents the core spins from rotating freely commensurate with the applied field, thereby leading to large observed coercivities. The first few layers of the NiO shell just surrounding the Ni core act as the pinning layers, whereas at the surface, the spins are uncompensated, misaligned, and without any magnetic order. It is these randomly oriented spins that align with difficulty with increasing field and give rise to the nonsaturating component of magnetization.

It is interesting to note that the magnetization of the annealed samples in both 0.1 M [Fig. 6(a)] and 0.5 M [Fig. 7(a)] cases is one order of magnitude higher than that of the respective as-prepared samples. The higher magnetization values are due to the increase of Ni volume fraction in the samples. This is clearly reflected in the XRD peaks at 2θ values of 44.5° and 51.85°. The increased Ni content enables ferromagnetic ordering to occur and hence leads to a larger particle moment.

2. Low magnetization values of as-prepared sample

We now turn our attention toward the question of why the as-prepared sample shows such a weak magnetic behavior. Figure 8(a) shows a model unit cell of tetragonal Ni with lattice parameters $a=4.920$ Å and $c=5.355$ Å. The nearest-

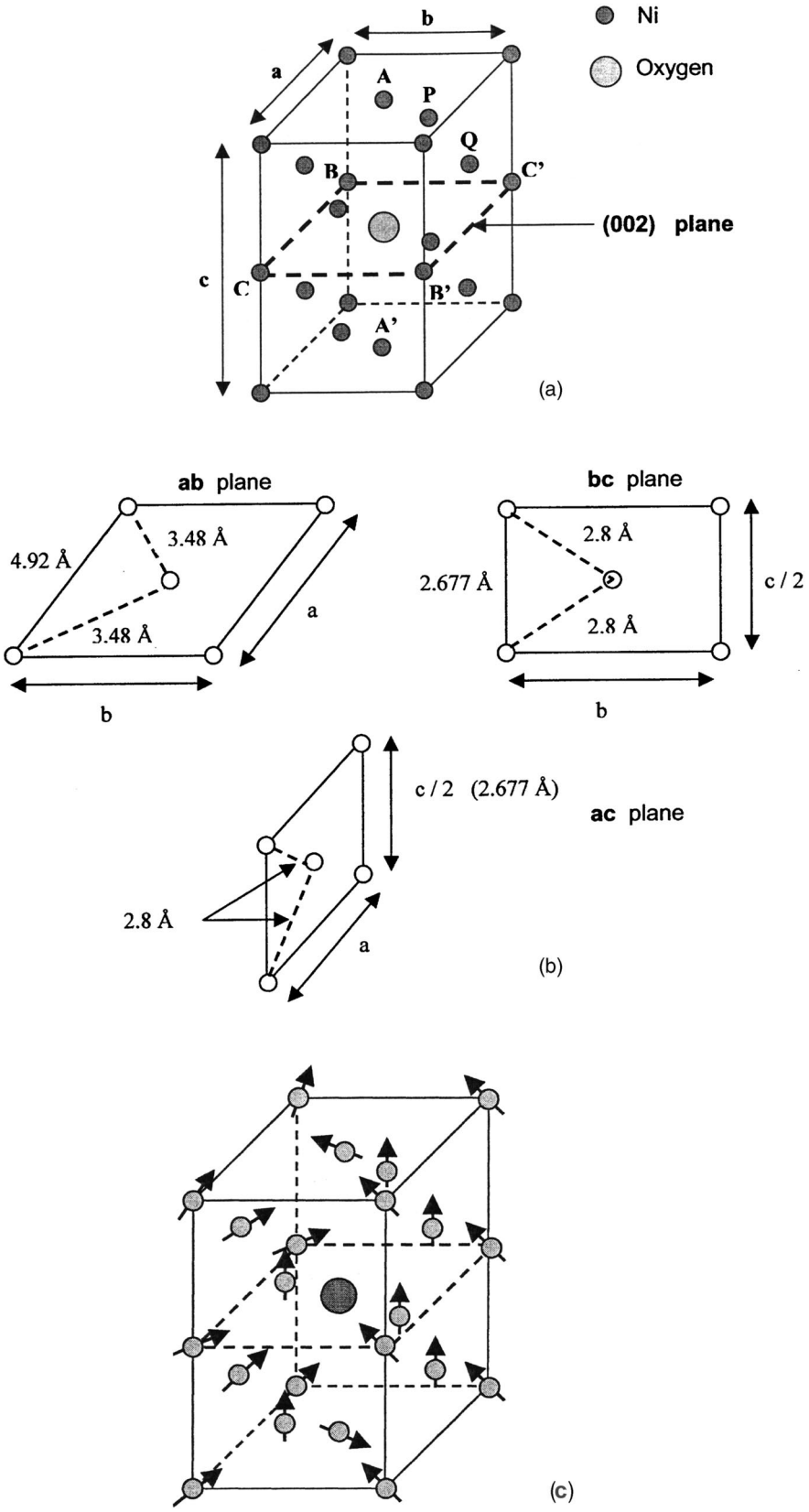

FIG. 8. (a) A model unit cell of tetragonal Ni with an oxygen atom at the center of the (002) plane. (b) Nearest-neighbor distances of Ni atoms in the *ab*, *bc*, and *ac* planes. (c) Orientation of Ni spins in the tetragonal unit cell.

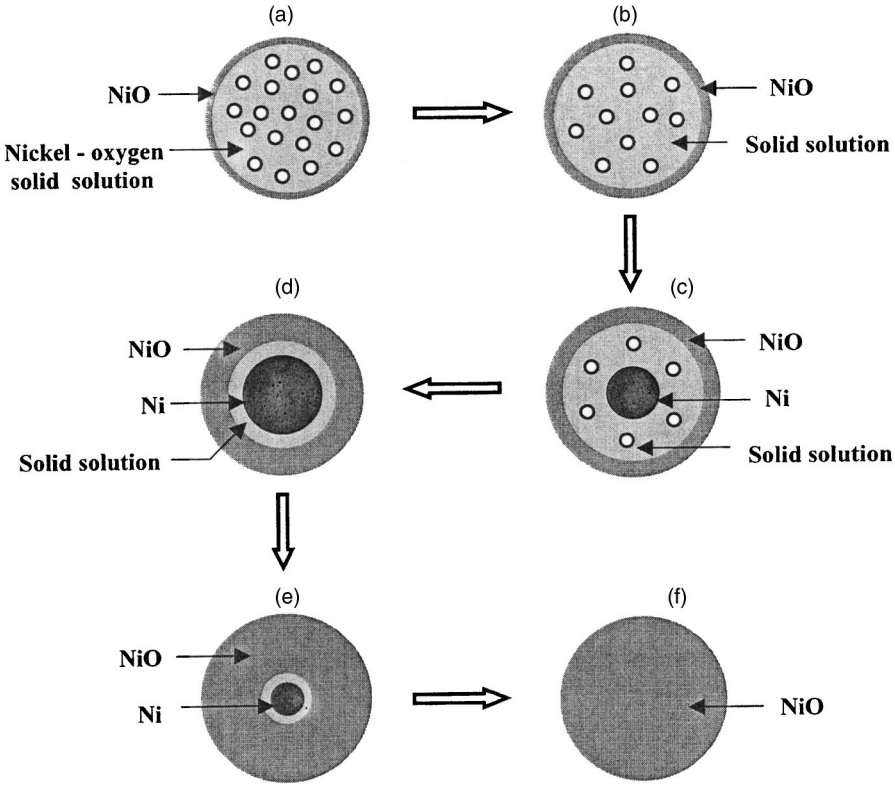

FIG. 9. The proposed model showing the transformation of a Ni nanoparticle from tetragonal to the fcc structure and final conversion to NiO. The small circles indicate dissolved oxygen.

neighbor distances of Ni atoms in *ab*, *bc*, and *ac* planes are pictorially represented in Fig. 8(b). In the absence of the (002) plane, the spin alignment of the Ni atoms remains perfectly ferromagnetic because the Ni atoms then stay arranged in their usual fcc crystal structure. The small separation between the atoms causes sufficient overlap of their 3*d* electronic wave functions due to which the Heisenberg exchange mechanism becomes effective and aligns the Ni atoms ferromagnetically.

The situation changes completely when the fcc unit cell gets strained and becomes tetragonal with the incorporation of an oxygen atom in the (002) plane [Fig. 8(a)]. The Ni atoms marked A and A′ are closest (2.677 Å) to the oxygen atom. Hence each one of them readily donates one 4*s* electron to the O atom, so that, the O atom becomes an O^{2-} ion with its 2*p* orbitals completely filled, i.e., having six electrons. The oxygen ion then interacts via its filled *p* orbitals with three pairs of Ni atoms marked as A and A′, B and B′, and C and C′ in Fig. 8(a), with each atom of a pair situated on opposite sides of the O ion. An interaction between the spin moments of the atoms in any pair proceeds by an overlap of the 3*d* orbitals of these atoms with any of the 2*p* orbitals of the O ion.

Such an indirect exchange interaction between two 3*d* magnetic atoms mediated by a completely filled, intervening anion *p* orbital is called "superexchange" interaction. It couples the magnetic atoms antiferromagnetically and is strongest in structures where the three ions are collinear. The superexchange interaction between the spin moments of atomic pairs B and B′ and C and C′ in the (002) plane and the pair A and A′ in the vertical plane tends to align the atoms in these pairs antiferromagnetically. However as the nearest-neighbor distance (2.677 Å) between Ni atoms in both *bc* and *ac* planes is far smaller than the Ni-O distance (3.48 Å) in the *ab* plane, there remains strong ferromagnetic direct exchange between the Ni atoms on these planes (*bc* and *ac*). This prevents the indirect superexchange interaction from being fully effective. As a result the atom pairs A and A′, B and B′, or C and C′ are not perfectly antiferromagnetically aligned. However the superexchange interaction is still strong enough to dislodge the spin moments of A′, B′, or C′ from their usual ferromagnetic alignment and make them point in the directions shown [Fig. 8(c)]. This in turn, affects the spin orientation of atoms like *P* and *Q*, which are situated at the centers of faces in the *bc* and *ac* planes and are the nearest neighbors of A′, B′, or C′.

The spin moments of these atoms can neither point in their original direction nor can they adopt the spin direction of the atoms A′, B′, or C′. Instead they point in an intermediate direction resulting in a complete disruption of the usual ferromagnetic alignment in the unit cell. Each particle, therefore, has a partly frustrated spin configuration with spins of Ni atoms pointing in noncollinear directions as shown in Fig. 8(c).[1] Such a state is responsible for the low values of magnetization of the as-prepared sample, where the concentration

[1]This picture attempts to depict the simultaneous occurrence of two diametrically opposite behaviors—itinerant and localized—of the 3*d* electrons of a transition metal ferromagnet. While the itinerant behavior of these electrons is used for describing the ferromagnetism of transition metals, their localized nature explains superexchange interactions in insulating oxides of the metals. A juxtaposition of these two completely contrasting electronic traits in the same system, therefore, requires reconciliation between the itinerant electron model and the local moment picture. This, however, may indeed become possible since at present there is no theory on

of dissolved oxygen is high enough to lead to the above-described state in the entire particle. It yields a net particle moment too small to be thermally stable, making the sample exhibit relaxation features. It must be remarked that the dissolved oxygen first reduces the moment, which, due to thermal agitation, is very hard to align with the field and yields a linear response up to 14 kOe at 300 K, and a relatively low magnetization at this field, still far away from saturation. It would be interesting to numerically model the ground-state spin configuration of the unit cell.

D. Analysis on the basis of the proposed model

In order to explain the surprising and apparently conflicting features of the XRD patterns and magnetization (*M-H*) curves of our samples, we have proposed a model as shown in Fig. 9. A brief recapitulation of the main features of XRD and magnetization measurements will not be out of place here. These are (a) XRD pattern of as-prepared sample does not correspond to fcc Ni. We propose that it is tetragonal Ni, stabilized by dissolved oxygen in the Ni lattice. (b) The fcc Ni peaks appear on annealing. (c) The as-prepared sample has very low magnetization values and is possibly super paramagnetic in nature. (d) Samples annealed at 573 and 773 K are ferromagnetic with high values of magnetization. From the analysis of these results, we put forward the following mechanism, which elucidates the evolution of fcc Ni and its final transformation to NiO.

Figure 9(a) shows a particle of the as-prepared sample, which is an interstitial solid solution of Ni and oxygen, with oxygen atoms (indicated by small circles) situated at the center of the (002) planes [Fig. 8(a)]. A thin SSO layer of NiO is shown encapsulating the particle since the sample has been prepared in ambient atmosphere. Hence the surface-passivation layer of NiO is inevitable. As explained in Sec. III C 2, the dissolved oxygen atoms play the central role in drastically reducing the magnetization of the as-prepared sample by giving rise to a certain degree of frustration of the Ni moments. Furthermore, the low molarity (0.1 M) of the $NiCl_2$ solution in the present study results in particles with low Ni content and small size (20 nm) as estimated from TEM micrographs. This, coupled with the random orientation of the spins of Ni atoms in a particle, causes the net magnetic moment of each particle to be quite small. Therefore relaxation of particle moment occurs and the ensemble of particles acts as magnetic entities with completely disordered and unrelated individual moments.

Figure 9(b) shows an intermediate stage. There is a decrease in the number of dissolved oxygen atoms and a slight increase in the thickness of the NiO shell. As thermal treatment results in mobility of the dissolved oxygen, the O atoms migrate outward from the oxygen-rich solid solution toward the NiO shell, which is nonstoichiometric and deficient in oxygen, leading to an increase in the thickness of the shell. This is probably the situation in 473 K annealed sample (XRD not shown).

Figure 9(c) represents the 573 K annealed sample. A substantial reduction in the number of dissolved oxygen atoms leads to the release of strain from the Ni lattice and the return of Ni back to fcc structure. Hence a clear appearance of a fcc Ni core is shown. However, since dissolved oxygen is still present, the tetragonal structure of Ni also remains. This sample thus shows the simultaneous existence of Ni in fcc and tetragonal phases. The formation of the fcc phase gives rise to the large increase in magnetic moment, as observed in the *M-H* measurements.

Figure 9(d) shows that on further annealing, the dissolved oxygen reduces down to an insignificant amount, leading to the formation of a large pure FCC Ni core (perfectly ferromagnetically ordered) and hence further enhanced values of magnetic moment. As expected, the sample behaves ferromagnetically. This is the situation in the 773 K annealed sample where FCC Ni peaks are observed along with NiO peaks. An exchange interaction between the NiO surface layer (now stoichiometric) and Ni core as explained in Sec. III C 1, gives rise to a large coercivity of 289 Oe.

An efficient reaction with oxygen from air occurs on annealing at further higher temperatures, resulting in the thickening of the NiO shell and reduction of size of the Ni core. As the oxygen-rich Ni solid solution is very nearly absent, there exists a gradient of oxygen presence as one moves inward from the shell toward the core. Since the outer region has sufficient oxygen, the oxygen from outside diffuses through the NiO layer, comes toward the oxygen deficient region, and reacts with the Ni atoms of the core, forming NiO. This increases the NiO dimensions and reduces the core dimensions [Fig. 9(e)] until, finally, at 973 K, the sample is completely converted to NiO [Fig. 9(f)].

IV. CONCLUSION

Fine particles of oxide-coated Ni have been synthesized using the borohydride reduction method. The XRD patterns have been indexed as Ni in a tetragonal crystal structure. The DTA/TGA profiles corroborate the proposition that tetragonal Ni is formed by the incorporation of dissolved oxygen atoms. The low magnetization values of the as-prepared sample have been attributed to an antiferromagnetic superexchange interaction between some of the Ni atoms mediated by the dissolved oxygen atoms in the Ni lattice. The appearance of FCC Ni peaks in the XRD patterns of annealed samples and their subsequent ferromagnetic behaviour has been analyzed and consistently explained on the basis of a proposed phenomenological model.

finite temperature metallic magnetism, which is generally accepted. Rather a judicious combination of both localized and itinerant models is necessary.[41] This can be realized by assuming that the 3*d* electrons do migrate but that they spend a large amount of their time close to the Ni ionic sites.[42] This would then impart to the 3*d* electrons a flavor of localized behavior. We propose that it is this "localized contribution" to the Ni moment that may well take part in superexchange interactions, given the presence of dissolved oxygen atoms and the structural model explained in Figs. 8(a) and 8(b). Although the proposed combination of "direct exchange" and "indirect superexchange" interactions between the Ni atoms lucidly explains the magnetic properties of the as-prepared sample in a qualitative manner, detailed theoretical calculations are needed for quantification of the results.

ACKNOWLEDGMENTS

One of the authors (V. S.) would like to thank JSPS for financial support for his short visit to Nagoya University. J. A. De Toro acknowledges financial support from the sixth European Community Framework Programme (MEIF-CT-2003–500580).

*Corresponding author. Email address: veeturi@phy.iitkgp.ernet.in
†Present address: Department of Physics, University of Liverpool, Oliver Lodge Laboratory, Liverpool L69 7ZE, United Kingdom

[1] J. L. Dorman, D. Fiorani, and E. Tronc, Adv. Chem. Phys. **98**, 283 (1997).
[2] J. L. Dorman and D. Fiorani, *Magnetic Properties of Fine Particles*, edited by J. L. Dorman and D. Fiorani (North Holland, Amsterdam, 1992).
[3] Mary Beth Stearns and Yuanda Cheng, J. Appl. Phys. **75**, 6894 (1994).
[4] J. L. Dorman *et al.*, J. Magn. Magn. Mater. **187**, L139–144 (1998).
[5] R. H. Kodama, A. E. Berkowitz, E. J. McNiff Jr., and S. Foner, Phys. Rev. Lett. **77**, 394 (1996).
[6] E. E. Carpenter, J. A. Sims, J. A. Wienmann, W. L. Zhou, and C. J. Connor, J. Appl. Phys. **87**, 5615 (2000).
[7] S. H. Liou, S. Huang, E. Climek, R. D. Kirby, and Y. D. Yao, J. Appl. Phys. **85**, 4334 (1999).
[8] C. Ballesteros, A. Zern, A. Garcia-Escorial, A. Hernando, and J. M. Rojo, Phys. Rev. B **58**, 89 (1998).
[9] P. Muniz, J. A. De. Toro, and J. M. Riveiro, Phys. Rev. B **66**, 104101 (2002).
[10] E. D. Biasi, C. A. Ramos, R. D. Zysler, and H. Romero, Phys. Rev. B **65**, 144416 (2002).
[11] Jose Vargas, C. Ramos, R. D. Zysler, and H. Romero, Physica B **320**, 178 (2002).
[12] L. Del. Bianco, D. Fiorani, A. M. Testa, E. Bonetti, L. Savini, and S. Signoretti, J. Magn. Magn. Mater. **262**, 128 (2003).
[13] L. Savini, E. Bonetti, L. D. Bianco, L. Pasquini, L. Signorini, M. Coisson, and V. Selvaggini, J. Magn. Magn. Mater. **262**, 56 (2003).
[14] F. Bodker, S. Morup, S. W. Charles, and S. Linderoth, J. Magn. Magn. Mater. **196–197**, 18 (1999).
[15] J. C. Jenardin, A. L. Brandl, M. Knobel, P. Panissod, A. B. Pakhomov, H. Liu, and X. X. Zhang, Phys. Rev. B **65**, 064422 (2002).
[16] F. C. Fonseca, G. F. Goya, R. F. Jardin, R. Muecillo, N. L. V. Carreno, E. Longo, and E. R. Leite, Phys. Rev. B **66**, 104406 (2002).
[17] T. Sekino, T. Nakajima, and K. Niihara, Mater. Lett. **29**, 165 (1996).
[18] T. Sekino, T. Nakajima, S. Ue da, and K. Niihara, J. Am. Ceram. Soc. **80**, 1139 (1997).
[19] L. Del. Bianco, A. Hernando, M. Multigner, C. Prados, J. C. Sanchez-Lopez, A. Fernandez, C. F. Conde, and A. Conde, J. Appl. Phys. **84**, 2189 (1998).
[20] H. Kisker, T. Gessmann, R. Wurschum, H. Kronmuller, and H. E. Schaefer, Nanostruct. Mater. **6**, 925 (1995).
[21] H. Y. Kai, thesis, University of Amsterdam, 1993.
[22] S. Gangopadhyay, G. C. Hadjipanayis, B. Dale, C. M. Sorensen, K. J. Klabunde, V. Papaefthymiou, and A. Kostikas, Phys. Rev. B **45**, 9778 (1992).
[23] J. P. Chen, C. M. Sorensen, K. J. Klabunde, and G. C. Hadjipanayis, Phys. Rev. B **51**, 11527 (1995).
[24] M. Respaud *et al.*, Phys. Rev. B **57**, 2925 (1998).
[25] Y. D. Yao, Y. Y. Chen, M. F. Tai, D. H. Wang, and H. M. Lin, Mater. Sci. Eng. **217–218**, 281 (1996).
[26] R. Karmhag, G. A. Niklasson, and M. Nygren, J. Appl. Phys. **89**, 3012 (2001).
[27] S. A. Makhlouf, F. T. Parker, F. E. Spada, and A. E. Berkowitz, J. Appl. Phys. **81**, 5561 (1997).
[28] R. H. Kodama, S. A. Makhlouf, and A. E. Berkowitz, Phys. Rev. Lett. **79**, 1393 (1997).
[29] F. Bodker, M. F. Hansen, C. Bender Koch, and S. Morup, J. Magn. Magn. Mater. **221**, 32 (2000).
[30] Liu *et al.*, J. Electrochem. Soc. **143**, 124 (1996).
[31] G. N. Glavee, K. J. Klabunde, C. M. Sorensen, and G. C. Hadjipanayis, Langmuir **10**, 4726 (1994).
[32] D. A. Van Leeuwen, J. M. Van Ruitenbeck, L. J. De Jonyh, A. Ceriotti, G. Pacchioni, O. D. Haberlen, and R. Rosch, Phys. Rev. Lett. **73**, 1432 (1994).
[33] G. N. Glavee, K. J. Klabunde, C. M. Sorensen, and G. C. Hadjipanayis, Inorg. Chem. **32**, 474 (1994).
[34] J. Park and J. Cheon, J. Am. Chem. Soc. **123**, 5743 (2001).
[35] S. Ram and P. S. Frankwickz, Phys. Status Solidi A **188**, 1129 (2001).
[36] J. Legrand, A. Taleb, S. Gota, M. J. Guittet, and C. Petit, Langmuir **18**, 4131 (2002).
[37] Aparna Roy, V. Srinivas, S. Ram, J. A. De. Toro, and J. M. Riveiro, J. Appl. Phys. **96**, 6782 (2004).
[38] X-ray Powder Diffraction file JCPDS-ICDD (Joint Committee on Powder Diffraction Standards—International Centre for Diffraction Data, Swarthmore, PA) 04-850 Ni.
[39] Jorg Loffler, H. Van. Swygenhoven, W. Wagner, J. Meier, B. Doudin, and J. Ph. Ansermet, Nanostruct. Mater. **9**, 523 (1997).
[40] R. H. Kodama, S. A. Makhlouf, and A. E. Berkowitz, Phys. Rev. Lett. **79**, 1393 (1997).
[41] The following citations from the book *Metallic Magnetism*, edited by H. Capellmann, (Springer-Verlag, Germany 1987) depicting the inadequacy of the itinerant electron model particularly at finite temperatures, further corroborates this point: (a) on p. 187: "With increasing temperature, transition metals show more and more local moment characteristics while the itinerant or delocalized features seem to become less important. For example in Fe, Co and Ni, the magnetization curves as a function of temperature resemble closely Brillouin curves which would follow from a localized electron description." (b) On p. 61: "Even when considering the 3d electrons to be itinerant, local magnetic moments might exist at the lattice sites."
[42] David Jiles, *Introduction to Magnetism and Magnetic Materials*, (Chapman and Hall, London 1991) p. 189.